Articles

Synthesis and Electronic Spectroscopy of Luminescent Cyclometalated Platinum−Anthracenyl Complexes

Jian Hu,[‡] Ronger Lin,[‡] John H. K. Yip,*[,‡] Kwok-Yin Wong,[†] Dik-Lung Ma,[†] and Jagadese J. Vittal[‡]

Department of Chemistry, National University of Singapore, 3 Science Drive 3, Singapore, 117543, and Department of Applied Biology and Chemical Technology, The Hong Kong Polytechnic University, Hung Hom, Kowloon, Hong Kong SAR, People's Republic of China

Received July 16, 2007

Dicyclometalated complexes *syn*- and *anti*-$[Pt_2(L)_2(PAnP\text{-}H_2)](OTf)_2$ (**Pt_2**) are synthesized from reactions of 9,10-bis(diphenylphosphino)anthracene (PAnP) and $Pt(L)(OTf)_2$ (L = diphosphines, OTf = CF_3SO_3). Because of metal perturbation on the electronic structure of the anthracenyl ring, the $^1B_{2u}^- \leftarrow {}^1A_g$ transition, which is forbidden in anthracene, is observed in the electronic spectra of **Pt_2**. The complexes display fluorescence arising from the ligand-centered S_1 excited state. No significant heavy atom effect is observed in the **Pt_2** complexes. To understand the effect of the number of Pt ions on the extent of perturbation, a mononuclear analogue, $[Pt(dppe)(PAn\text{-}H)]ClO_4$ (PAn = 9-diphenylphosphinoanthracene), is prepared and its spectroscopy studied.

Introduction

Platinum(II) complexes has assumed an important position in inorganic spectroscopy since the seminal work of Ballhausen,[1a] Gray,[1b] Martin,[1c−e] Patterson,[1f] and others on $PtCl_4^{2-}$ and related complexes in the 1960s. The last two decades have witnessed an exponential growth in studies on the spectroscopy, photophysics, and photochemistry of luminescent platinum complexes,[2−20] chiefly because of their applications in important areas such as solar energy conversion,[8,14,20b] photocatalysis,[2,17e,19] sensing,[3−5,17b−d,18] biolabeling,[16b] and OLED.[9−12,17d,20a] The most extensively studied systems are the ones that contain polypyridine ligands such as bipyridine,[13,14,18a,b,19a,20] terpyridine,[2,4,16,17c] and their various

* Correspondence author. E-mail: chmyiphk@nus.edu.sg. Fax: 65-67791691.

‡ National University of Singapore.

† The Hong Kong Polytechnic University.

(1) (a) Gray, H. B.; Ballhausen, C. J. *J. Am. Chem. Soc.* **1963**, *85*, 260. (b) Basch, H.; Gray, H. B. *Inorg. Chem.* **1967**, *6*, 365. (c) Martin, D. S. J.; Lenhardt, C. A. *Inorg. Chem.* **1964**, *3*, 1368. (d) Martin, D. S. J.; Tucker, M. A.; Kassman, A. J. *Inorg. Chem.* **1965**, *4*, 1682. (e) Martin, D. S. J.; Tucker, M. A.; Kassman, A. *J. Inorg. Chem.* **1966**, *5*, 1298. (f) Patterson, H. H.; Harrison, T. G.; Belair, R. *Inorg. Chem.* **1976**, *15*, 1461.

(2) (a) Yang, Y.; Zhang, D.; Wu, L.-Z.; Chen, B.; Zhang, L.-P.; Tung, C.-H. *J. Org. Chem.* **2004**, *69*, 4788. (b) Zhang, D.; Wu, L.-Z.; Zhou, L.; Han, X.; Yang, Q.-Z.; Zhang, L.-P.; Tung, C.-H. *J. Am. Chem. Soc.* **2004**, *126*, 3440.

(3) (a) Buss, C. E.; Anderson, C. E.; Pomije, M. K.; Lutz, C. M.; Britton, D.; Mann, K. R. *J. Am. Chem. Soc.* **1998**, *120*, 7783. (b) Buss, C. E.; Mann, K. R. *J. Am. Chem. Soc.* **2002**, *124*, 1031. (c) Zhang, H.; Sun, Y.; Ye, K.; Zhang, P.; Wang, Y. *J. Mater. Chem.* **2005**, *15*, 3181. (d) Kunugi, Y.; Mann, K. R.; Miller, L. L.; Exstrom, C. L. *J. Am. Chem. Soc.* **1998**, *120*, 589.

(4) (a) Tang, W.-S.; Lu, X.-X.; Wong, K. M.-C.; Yam, V. W.-W. *J. Mater. Chem.* **2005**, *15*, 2714. (b) Lo, H.-S.; Yip, S.-K.; Wong, K. M.-C.; Zhu, N.; Yam, V. W.-W. *Organometallics* **2006**, *25*, 3537. (c) Wong, K. M.-C.; Tang, W.-S.; Lu, X.-X.; Zhu, N.; Yam, V. W.-W. *Inorg. Chem.* **2005**, *44*, 1492. (d) Peyratout, C. S.; Aldridge, T. K.; Crites, D. K.; McMillin, D. R. *Inorg. Chem.* **1995**, *34*, 4484. (e) Wadas, T. J.; Wang, Q.-M.; Kim, Y.-J.; Flaschenreim, C.; Blanton, T. N.; Eisenberg, R. J. *Am. Chem. Soc.* **2004**, *126*, 16841. (f) Cusumano, M.; Di Pietro, M. L.; Giannetto, A. *Inorg. Chem.* **1999**, *38*, 1754.

(5) (a) Liu, H.-Q.; Cheung, T.-C.; Che, C.-M. *Chem. Commun.* **1996**, 1039. (b) Wu, L.-Z.; Cheung, T.-C.; Che, C.-M.; Cheung, K.-K.; Lam, M. H. W. *Chem. Commun.* **1998**, 1127. (c) Wong, K.-H.; Chan, M. C.-W.; Che, C.-M. *Chem.−Eur. J.* **1999**, *5*, 2845. (d) Siu, P. K. M.; Lai, S.-W.; Lu, W.; Zhu, N.; Che, C.-M. *Eur. J. Inorg. Chem.* **2003**, 2749. (e) Che, C.-M.; Zhang, J.-L.; Lin, L.-R. *Chem. Commun.* **2002**, 2556.

(6) (a) Chan, C.-W.; Cheng, L.-K.; Che, C.-M. *Coord. Chem. Rev.* **1994**, *132*, 87. (b) Drew, S. M.; Janzen, D. E.; Buss, C. E.; MacEwan, D. I.; Dublin, K. M.; Mann, K. R. *J. Am. Chem. Soc.* **2001**, *123*, 8414.

(7) (a) Yip, J. H. K.; Suwarno; Vittal, J. J. *Inorg. Chem.* **2000**, *39*, 3537. (b) Williams, J. A. G.; Beeby, A.; Davies, E. S.; Weinstein, J. A.; Wilson, C. *Inorg. Chem.* **2003**, *42*, 8609.

(8) (a) Geary, E. A. M.; Yellowlees, L. J.; Jack, L. A.; Oswald, I. D. H.; Parsons, S.; Hirata, N.; Durrant, J. R.; Robertson, N. *Inorg. Chem.* **2005**, *44*, 242. (b) Islam, A.; Sugihara, H.; Hara, K.; Singh, L. P.; Katoh, R.; Yanagida, M.; Takashi, Y.; Murata, S.; Arakawa, H.; Fujihashi, G. *Inorg. Chem.* **2001**, *40*, 5371. (c) McGarrah, J. E.; Kim, Y.-J.; Hissler, M.; Eisenberg, R. *Inorg. Chem.* **2001**, *40*, 4510.

(9) (a) Lu, W.; Mi, B.-X.; Chan, M. C. W.; Hui, Z.; Zhu, N.; Lee, S.-T.; Che, C.-M. *Chem. Commun.* **2002**, 206. (b) Sotoyama, W.; Satoh, T.; Sawatari, N.; Inoue, H. *Appl. Phys. Lett.* **2005**, *86*, 153505. (c) Lu, W.; Mi, B.-X.; Chan, M. C. W.; Hui, Z.; Che, C.-M.; Zhu, N.; Lee, S.-T. *J. Am. Chem. Soc.* **2004**, *126*, 4958.

(10) (a) Lin, Y.-Y.; Chan, S.-C.; Chan, M. C. W.; Hou, Y.-J.; Zhu, N.; Che, C.-M.; Liu, Y.; Wang, Y. *Chem.−Eur. J.* **2003**, *9*, 1263. (b) Nishida, J.-I.; Maruyama, A.; Iwata, T.; Yamashita, Y. *Chem. Lett.* **2005**, *34*, 592. (c) Kwok, C.-C.; Ngai, H. M. Y.; Chan, S.-C.; Sham, I. H. T.; Che, C.-M.; Zhu, N. *Inorg. Chem.* **2005**, *44*, 4442.

(11) (a) Baldo, M. A.; O'Brien, D. F.; You, Y.; Shoustikov, A.; Sibley, S.; Thompson, M. E.; Forrest, S. R. *Nature* **1998**, *395*, 151. (b) O'Brien, D. F.; Baldo, M. A.; Thompson, M. E.; Forrest, S. R. *Appl. Phys. Lett.* **1999**, *74*, 442. (c) Kwong, R. C.; Sibley, S.; Dubovoy, T.; Baldo, M. A.; Forrest, S. R.; Thompson, M. E. *Chem. Mater.* **1999**, *11*, 3709. (d) Chang, S.-Y.; Kavitha, J.; Li, S.-W.; Hsu, C.-S.; Yeh, Y.-S.; Chou, P.-T.; Lee, G.-H.; Carty, A. J.; Tao, Y.-T.; Chien, C.-H. *Inorg. Chem.* **2006**, *45*, 137. (e) Cleave, V.; Yahioglu, G.; Barny, P. L.; Friend, R. H.; Tessler, N. *Adv. Mater.* **1999**, *11*, 285. (f) Ma, B.; Li, J.; Djurovich, P. I.; Yousufuddin, M.; Bau, R.; Thompson, M. E. *J. Am. Chem. Soc.* **2005**, *127*, 28.

10.1021/om700706r CCC: $37.00
Publication on Web 11/27/2007

derivatives.[5−10,17d,18c,19c] Among them, cyclometalated Pt complexes have been commanding a lot of attention mainly because of their relatively long-lived emissive excited states and tunable electronic and molecular properties.[5,7,9,12,17] Because of their close intraligand $\pi-\pi^*$ and metal-to-ligand charge-transfer (MLCT) excited states, the excited-state properties of the complexes are rather sensitive to intermolecular metal−metal, $\pi-\pi$ interactions and medium effects.

While there are a lot of studies on Pt complexes of polypyridine-type ligands, complexes of alternant aromatic hydrocarbons (AAH) such as anthracene and pyrene have not received much attention.[12b,17b,21] Given the fact that many AAH are well-known organic chromophores, it is envisioned that metalated AAH could be developed into a class of new luminescent organometallic materials with different photophysical properties and chemical reactivity. It is reasonable to expect the photophysics of metalated AAH will be very different from other cyclometalates. For instance, a salient feature of AAH is that due to the large exchange interaction K, the energy separation between the singlet and triplet excited states ($\sim 2K$) is large. Accordingly, the intersystem crossing in metalated AAH is dependent on the nature of the metal attached to the rings and its perturbation on the electronic structures of the AAH. Recently, applications of metal−π-conjugated systems such as metal−acetylides as optoelectronic materials have been actively explored. Metal−AAH complexes could be another direction in the endeavor. The design of metal−AAH-based materials requires an understanding of how metals interact with the extended π-conjugated systems of the organic molecules, which can be garnered by studying the electronic spectroscopy of the complexes.

Our laboratory has recently reported the syntheses of a diphosphine 9,10-bis(diphenylphosphino)anthracene (PAnP) (Scheme 1).[22a] A special feature of the ligand is its chromophoric anthracenyl backbone, which can impart luminescence to its complexes.[22] To further explore the coordination chemistry of PAnP, we studied its reactions with $[Pt^{II}(L)(OTf)_2]$ (L = bis(diphenylphosphino)methane (dppm), 1,2-bis(diphenylphosphino)ethane (dppe), 1,3-bis(diphenylphosphino)propane (dppp)) (Scheme 1). Our results show that reactions produce dicyclometalated platinum complexes *syn*- and *anti*-$[Pt_2(L)_2(PAnP\text{-}H_2)](OTf)_2$ (**Pt_2**). The spectroscopy and photophysics of **Pt_2** provide insights into the interactions between metal and alternant aromatic hydrocarbons. To understand the effect of the number of Pt ions on the extent of perturbation, a mononuclear analogue, $[Pt(dppe)(PAn\text{-}H)]ClO_4$ (**4**) (PAn = 9-diphenylphosphinoanthracene), has been prepared and its spectroscopy studied. Reported in this paper is our effort to understand the electronic structures of the cyclometalated platinum−anthracenyl complexes.

Experimental Section

General Methods. All syntheses were carried out in a N_2 atmosphere. All the solvents used for synthesis and spectroscopic measurements were purified according to the literature procedures. $PtCl_2$ was obtained from Oxkem; bis(diphenylphosphino)methane (dppm), 1,2-bis(diphenylphosphino)ethane (dppe), 1,3-bis(diphenylphosphino)propane (dppp), *n*-butyllithium, 9-bromoanthracene, and 9,10-dibromoanthracene were purchased from Aldrich and used without further purification. 9,10-Bis(diphenylphosphino)anthracene (PAnP)[22a] and 9-(diphenylphosphino)anthracene (PAn)[23] were prepared according to the reported methods. $Pt(L)(OTf)_2$[24] were prepared *in situ* by reacting $Pt(L)Cl_2$ with 2 molar equiv of AgOTF in CH_3CN/CH_2Cl_2 based on modified literature methods.

Physical Measurements. The UV–vis absorption and room-temperature emission spectra of the complexes were recorded on a Shimadzu UV-1601 UV–visible spectrophotometer and a Perkin-Elmer LS-50B luminescence spectrometer, respectively. The emission quantum yields were measured with anthracene as standard. Solutions used for emission spectra and lifetime measurements were degassed by four freeze–pump–thaw cycles. NMR experiments were performed on a Bruker ACF 300, AMX500, or DRX500 spectrometer. All chemical shifts (δ) are reported in ppm and coupling

(12) (a) Ma, B.; Djurovich, P. I.; Thompson, M. E. *Coord. Chem. Rev.* **2005**, *249*, 1501. (b) Kui, S. C. F.; Sham, I. H. T.; Cheung, C. C. C.; Ma, C.-W.; Yan, B.; Zhu, N.; Che, C.-M.; Fu, W.-F. *Chem.−Eur. J.* **2007**, *13*, 417. (c) Adachi, C.; Baldo, M. A.; Forrest, S. R.; Lamansky, S.; Thompson, M. E.; Kwong, R. C. *Appl. Phys. Lett.* **2001**, *78*, 1622. (d) Brooks, J.; Babayan, Y.; Lamansky, S.; Djurovich, P. I.; Tsyba, I.; Bau, R.; Thompson, M. E. *Inorg. Chem.* **2002**, *41*, 3055. (e) Adamovich, V.; Brooks, J.; Tamayo, A.; Alexander, A. M.; Djurovich, P. I.; D'Andrade, B. W.; Adachi, C.; Forrest, S. R.; Thompson, M. E. *New J. Chem.* **2002**, *26*, 1171.

(13) (a) Connick, W. B.; Miskowski, V. M.; Houlding, V. H.; Gray, H. B. *Inorg. Chem.* **2000**, *39*, 2585. (b) Fleeman, W. L.; Connick, W. B. *Comments Inorg. Chem.* **2002**, *23*, 205. (c) Houlding, V. H.; Miskowski, V. M. *Coord. Chem. Rev.* **1991**, *111*, 145. (d) Lee, J. K.-W.; Ko, C.-C.; Wong, K. M.-C.; Zhu, N.; Yam, V. W.-W. *Organometallics* **2007**, *26*, 12. (e) Zhang, Y.; Ley, K. D.; Schanze, K. S. *Inorg. Chem.* **1996**, *35*, 7102. (f) Whittle, E. C.; Weinstein, J. A.; George, M. W.; Schanze, K. S. *Inorg. Chem.* **2001**, *40*, 4053.

(14) (a) McGarrah, J. E.; Eisenberg, R. *Inorg. Chem.* **2003**, *42*, 4355. (b) Geary, E. A. M.; Hirata, N.; Clifford, J.; Durrant, J. R.; Parsons, S.; Dawson, A.; Yellowlees, L. J.; Robertson, N. *Dalton Trans.* **2003**, 3757. (c) Hissler, M.; McGarrah, J. E.; Connick, W. B.; Geiger, D. K.; Cummings, S. D.; Eisenberg, R. *Coord. Chem. Rev.* **2000**, *208*, 115.

(15) (a) Silverman, E. E.; Cardolaccia, T.; Zhao, X.; Kim, K.-Y.; Haskins-Glusac, K.; Schanze, K. S. *Coord. Chem. Rev.* **2005**, *249*, 1491. (b) Pettijohn, C. N.; Jochnowitz, E. B.; Chuong, B.; Nagle, J. K.; Vogler, A. *Coord. Chem. Rev.* **1998**, *171*, 85–92. (c) Sarova, G. H.; Bokach, N. A.; Fedorov, A. A.; Berberan-Santos, M. N.; Kukushkin, V. Y.; Haukka, M.; da Silva, J. J. R. F.; Pombeiro, A. J. L. *Dalton Trans.* **2006**, 3798–3805. (d) Haskins-Glusac, K.; Ghiviriga, I.; Abboud, K. A.; Schanze, K. S. *J. Phys. Chem. B* **2004**, *108*, 4969. (e) Cooper, T. M.; Hall, B. C.; Mclean, D. G.; Rogers, J. E.; Burke, A. R.; Turnbull, K.; Weisner, A.; Fratini, A.; Liu, Y.; Schanze, K. S. *J. Phys. Chem. A* **2005**, *109*, 999. (f) Kim, K.-Y.; Liu, S.; Köse, M. E.; Schanze, K. S. *Inorg. Chem.* **2006**, *45*, 2509. (g) Zhang, K.; Hu, J.; Chan, K. C.; Wong, K. Y.; Yip, J. H. K. *Eur. J. Inorg. Chem.* **2007**, 384.

(16) (a) McMillin, D. R.; Moore, J. J. *Coord. Chem. Rev.* **2002**, *229*, 113–121. (b) Wong, K. M.-C.; Tang, W.-S.; Chu, B. W.-K.; Zhu, N.; Yam, V. W.-W. *Organometallics* **2004**, *23*, 3459.

(17) (a) Yersin, H.; Donges, D. *Top. Curr. Chem.* **2001**, *214*, 81. (b) Kui, S. C. F.; Chui, S. S.-Y.; Che, C.-M.; Zhu, N. *J. Am. Chem. Soc.* **2006**, *128*, 8297. (c) Kato, M. *Bull. Chem. Soc. Jpn.* **2007**, *80*, 287. (d) Lai, S.-W.; Che, C.-M. *Top. Curr. Chem.* **2004**, *241*, 27. (e) Shavaleev, N.; Adams, H.; Best, J.; Edge, R.; Navaratnam, S.; Weinstein, J. A. *Inorg. Chem.* **2006**, *45*, 9410.

(18) (a) Liu, H.-Q.; Peng, S.-M.; Che, C. M. *J. Chem. Soc., Chem. Commun.* **1995**, 509. (b) Lu, W.; Chan, M. C. W.; Zhu, N.; Che, C.-M.; He, Z.; Wong, K.-Y. *Chem.−Eur. J.* **2003**, *9*, 6155. (c) Che, C.-M.; Yang, M.; Wong, K.-H.; Chan, H.-L.; Lam, W. *Chem.−Eur. J.* **1999**, *5*, 3350.

(19) (a) Connick, W. B.; Gray, H. B. *J. Am. Chem. Soc.* **1997**, *119*, 11620. (b) Kalsbeck, W. A.; Gingell, D. M.; Malinsky, J. E.; Thorp, H. H. *Inorg. Chem.* **1994**, *33*, 3313. (c) Li, X.-H.; Wu, L.-Z.; Zhang, L.-P.; Tung, C.-H.; Che, C.-M. *Chem. Commun.* **2001**, 2280.

(20) (a) Chan, S.-C.; Chan, M. C. W; Wang, Y.; Che, C.-M.; Cheung, K.-K.; Zhu, N. *Chem.−Eur. J.* **2001**, *7*, 4180. (b) Paw, W.; Cummings, S. D.; Mansour, M. A.; Connick, W. B.; Geiger, D. K.; Eisenberg, R. *Coord. Chem. Rev.* **1998**, *171*, 125.

(21) (a) Yam, V. W.-W.; Cheung, K. L.; Yip, S. K.; Zhu, N. *Photochem. Photobiol. Sci.* **2005**, *4*, 149. (b) Osawa, M.; Hoshino, M.; Akita, M.; Wada, T. *Inorg. Chem.* **2005**, *44*, 1157. (c) Burdzinski, G. T.; Ramnauth, R.; Chisholm, M. H.; Gustafson, T. L. *J. Am. Chem. Soc.* **2006**, *128*, 6776.

(22) (a) Yip, J. H. K.; Prabhavathy, J. *Angew. Chem., Int. Ed.* **2001**, *40*, 2159. (b) Lin, R.; Yip, J. H. K.; Zhang, K.; Koh, L. L.; Wong, K.-Y.; Ho, K. P. *J. Am. Chem. Soc.* **2004**, *126*, 15852. (c) Zhang, K.; Prabhavathy, J.; Yip, J. H. K.; Koh, L. L.; Tan, G. K.; Vittal, J. J. *J. Am. Chem. Soc.* **2003**, *125*, 8452. (d) Lin, R.; Yip, J. H. K. *Inorg. Chem.* **2006**, *45*, 4423.

(23) Wesemann, J.; Jones, P. G.; Schomburg, D.; Heuer, L.; Schmutzler, R. *Chem. Ber* **1992**, *125*, 2187.

(24) (a) Anderson, G. K.; Davies, J. A.; Schoeck, D. J. *Inorg. Chim. Acta* **1983**, *76*, L251. (b) Fallis, S.; Anderson, G. K.; Rath, N. P. *Organometallics* **1991**, *10*, 3180. (c) Stang, P. J.; Cao, D. H.; Saito, S.; Arif, A. M. *J. Am. Chem. Soc.* **1995**, *117*, 6273.

Scheme 1

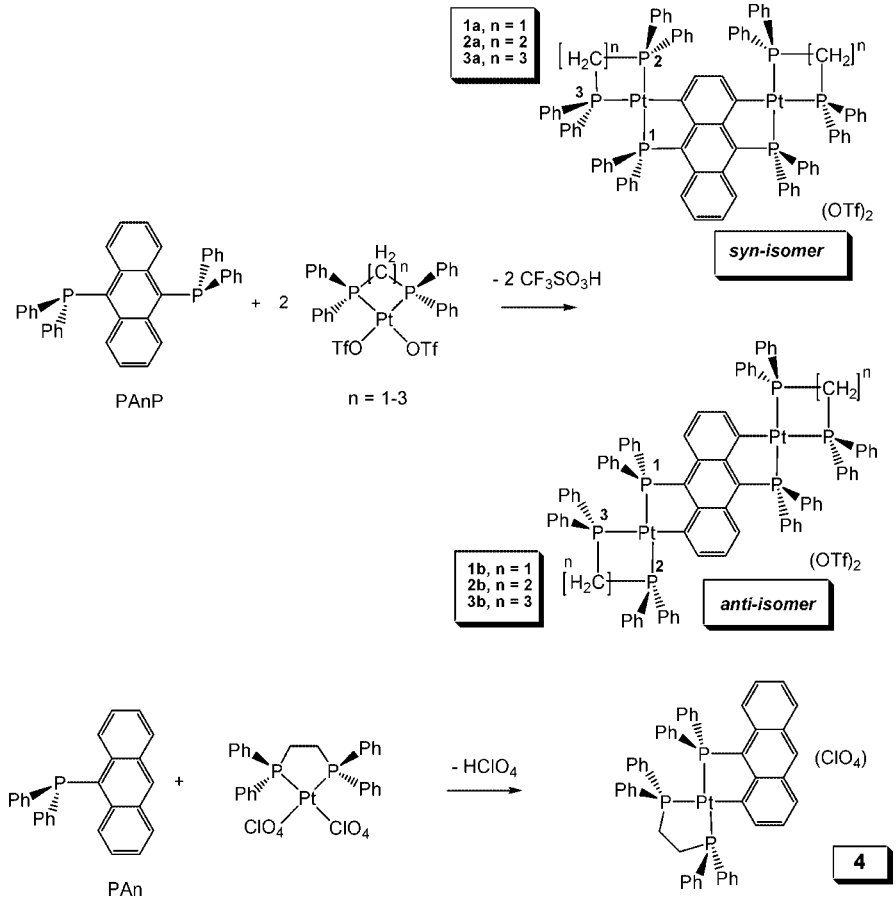

constants (J) in Hz. ^{1}H NMR chemical shifts are relative to tetramethylsilane; the resonance of residual protons of solvents was used as an internal standard. ^{31}P{^{1}H} NMR chemical shifts were relative to 85% H_3PO_4 in D_2O. Electrospray ionization mass spectra (ESI-MS) were measured on a Finnigan MAT 731 LCQ spectrometer. Elemental analyses of the complexes were carried out at the Elemental Analysis Laboratory in the National University of Singapore.

Emission Lifetime Measurements. The 77 K frozen glass (MeOH/EtOH = 1:4) emission spectra were recorded on a SPEX Fluorolog-2 model fluorescence spectrophotometer. Emission lifetime measurements were performed with a Quanta Ray DCR-3 pulsed Nd:YAG laser system (pulse output 355 nm, 8 ns). Error limits were estimated as follows: λ (±1 nm); τ (±10%); φ (±10%). The nanosecond emission lifetime measurements were performed by time-correlated single-photon counting techniques, using a Fluorocube fluorescence lifetime system equipped with a NanoLED source (HORIBA Jobin Yvon IBH). The decays were analyzed by means of DataStation software v2.3.

Molecular Orbital Calculations. The electronic structure of PAnP with all its phenyl rings replaced with H atoms was calculated using the SPARTAN semiempirical program SGI/R10K release 5.1.3 with geometry optimization. The model RHF/PM3 was used in the calculations.

X-ray Crystallography. The diffraction experiments were carried out on a Bruker AXS SMART CCD three-circle diffractometer with a sealed tube at 23 °C using graphite-monochromated Mo Kα radiation (λ = 0.71073 Å). The software used were SMART[25a] for collecting frames of data, indexing reflections, and determination of lattice parameters; SAINT[25a] for integration of intensity of reflections and scaling; SADABS[25b] for empirical absorption correction; and SHELXTL[25c] for space group determination, structure solution, and least-squares refinements on $|F|^2$. The crystals were mounted at the end of glass fibers (**1a**, **2a**, **2b**, **3b**, and **4**) or sealed in a capillary tube (**3a**) and used for the diffraction experiments. Anisotropic thermal parameters were refined for the rest of the non-hydrogen atoms. The hydrogen atoms were placed in their ideal positions. A brief summary of crystal data and experimental details is given in Table 1.

Syntheses of *syn-/anti*-[Pt$_2$(dppm)$_2$(PAnP-H$_2$)](OTf)$_2$ (1a,b). PAnP (33 mg, 0.060 mmol) was added to 40 mL of a CH_3CN/CH_2Cl_2 (1:1, v/v) solution of 2 molar equiv of Pt(dppm)(OTf)$_2$ (93 mg, 0.121 mmol), which was prepared *in situ*. The solution was stirred at room temperature overnight and then filtered. The filtrate was concentrated by rotaevaporation, and yellow products were precipitated by adding excess diethyl ether to the solution. Single crystals of **1a** suitable for X-ray diffraction studies were obtained from slow diffusion of Et_2O into a CH_2Cl_2 solution of the crude products. Attempts failed to purify **1b** from the mixture products. Total yield: 102 mg, 85%. Anal. Calcd (%) for **1a** ($C_{90}H_{70}F_6O_6P_6Pt_2S_2$): C, 54.00; H, 3.52. Found (%): C, 53.96; H, 3.66. ^{1}H NMR (300 MHz, δ/ppm) for **1a** (in CD_2Cl_2): 7.85–7.82 (m, 2H, $H_{5,8}$ of anthracenyl ring (An)), 7.74–7.67 (m, 8H, Ph), 7.53–7.25 (m, 38H, Ph and $H_{2,3}$ of An), 7.21–7.18 (m, 2H, $H_{6,7}$, An), 7.16–7.03 (m, 16H, Ph), 4.83–4.61 (m, 4H, CH_2). ^{31}P{^{1}H} NMR for **1a** and **1b**: see Table 2. ESI-MS (m/z): **1a** and **1b** 851.9 [M − 2OTf]$^{2+}$.

Syntheses of *syn-/anti*-[Pt$_2$(dppe)$_2$(PAnP-H$_2$)](OTf)$_2$ (2a,b). PAnP (33 mg, 0.060 mmol) was added to 40 mL of a CH_3CN/CH_2Cl_2 (1:1, v/v) solution of 2 molar equiv of Pt(dppe)(OTf)$_2$ (95 mg, 0.121 mmol), which was prepared *in situ*. The mixture was stirred at room temperature overnight and then filtered. The filtrate

(25) (a) *SMART & SAINT Software Reference Manuals*, version 4.0; Siemens Energy & Automation, Inc., Analytical Instrumentation: Madison, WI, 1996. (b) Sheldrick, G. M. *SADABS*: A Software for Empirical Absorption Correction; University of Gottingen: Gottingen, Germany, 1996. (c) *SHELXTL Reference Manual*, version 5.03; Siemens Energy & Automation, Inc., Analytical Instrumentation: Madison, WI, 1996.

Table 1. Crystal Data for 1a, 2a, 2b, 3a, 3b, and 4

	1a·Et_2O	**2a**·1.25 (CH_2Cl_2)0.5(Et_2O)	**2b**·$2CH_2Cl_2$	**3a**·$4.5CH_2Cl_2$	**3b**·$4CH_2Cl_2$	**4**·CH_2Cl_2
formula	$C_{94}H_{80}F_6O_7P_6Pt_2S_2$	$C_{95.25}H_{81.50}Cl_{2.50}F_6O_{6.50}P_6Pt_2S_2$	$C_{94}H_{78}Cl_4F_6O_6Pt_2S_2$	$C_{98.50}H_{87}Cl_9F_6O_6P_6Pt_2S_2$	$C_{98}H_{86}Cl_8F_6O_6P_6Pt_2S_2$	$C_{53}H_{44}Cl_3O_4P_3Pt$
cryst size (mm^3)	0.35 × 0.18 × 0.10	0.20 × 0.16 × 0.10	0.38 × 0.18 × 0.14	0.60 × 0.44 × 0.10	0.30 × 0.20 × 0.12	0.36 × 0.12 × 0.08
cryst syst	orthorhombic	monoclinic	monoclinic	monoclinic	triclinic	monoclinic
space group	*Pnma*	*P*2(1)/*c*	*C*2/*c*	*C*2/*c*	$P\bar{1}$	*P*2(1)/*n*
lattice params (Å, deg)	*a* = 29.212(2), *b* = 28.996(3), *c* = 12.2327(10) α = 90; *β* = 90; *γ* = 90	*a* = 15.4379(13), *b* = 19.4669(15), *c* = 33.992(3) α = 90; *β* = 90.347(2); *γ* = 90	*a* = 18.8456(8), *b* = 15.1930(6), *c* = 31.3809(12) α = 90; *β* = 94.382(1); *γ* = 90	*a* = 31.534(4), *b* = 19.080(2), *c* = 17.170(2) α = 90; *β* = 92.981(2); *γ* = 90	*a* = 11.4542(6), *b* = 14.2431(7), *c* = 16.5993(8) α = 69.655(1); *β* = 77.781(1); *γ* = 8 7.317(1)	*a* = 11.6283(5), *b* = 27.3240(12), *c* = 14.7234(6) α = 90; *β* = 91.099(1); *γ* = 90
V ($Å^3$)	10361.4(15)	10215.5(14)	8959.8(6)	10317(2)	2480.5(2)	4677.2(3)
Z	4	4	**4**	**4**	**1**	4
density(calc) (g/cm^3)	1.331	1.413	1.631	1.571	1.605	1.618
absorpcoeff (mm^{-1})	2.887	2.995	3.459	3.137	3.234	3.321
F(000)	4128	4318	4360	4844	1190	2272
total no. of reflns	71 720	58 873	31 201	36 309	32 769	32 708
index ranges	$-26 \le h \le 37$, $-37 \le k \le 34$, $-15 \le l \le 15$	$-18 \le h \le 17$, $-20 \le k \le 23$, $-40 \le l \le 40$	$-17 \le h \le 24$, $-19 \le k \le 19$, $-38 \le l \le 40$	$-37 \le$ h≤ 40, $-22 \le k \le 24$, $-22 \le l \le 22$	$-14 \le h \le 14$, $-18 \le k \le 18$, $-21 \le l \le 21$	$-14 \le h \le 14$, $-18 \le k \le 18$, $-21 \le l \le 21$
2*θ* range for data collection (deg)	3.12–55.00	3.56–50.00	3.62–55.00	3.40–55.00	2.68–55.00	2.98–55.00
no. of indep reflns	12 124 (R_{int} = 0.0828)	18 002 (R_{int} = 0.0925)	10 281 (R_{int} = 0.0464)	11 831 (R_{int} = 0.0486)	11 403 (R_{int} = 0.0461)	10 715 (R_{int} = 0.0525)
no. of params varied	532	804	552	487	634	582
final *R* indices[a]	R1 = 0.0566, wR2 = 0.1444	R1 = 0.0711, wR2 = 0.2016	R1 = 0.0508, wR2 = 0.1221	R1 = 0.0502, wR2 = 0.1344	R1 = 0.0455, wR2 = 0.1141	R1 = 0.0416, wR2 = 0.0868
goodness of fit (GOF)[b]	1.058	0.996	1.034	1.009	1.083	1.067
largest diff peak and hole (e·$Å^{-3}$)	1.463 and –1.611	1.784 and –1.526	1.802 and −1.217	1.220 and –0.825	1.727 and –1.759	1.567 and –1.396

[a] $R1 = (F_o| - |F_c)/(|F_o|)$; $wR2 = [w(F_o^2 - F_c^2)/w(F_o^4)]^{1/2}$. [b] $GOF = [(w(F_o^2 - F_c^2)^2/(n - p)]^{1/2}$. For all crystal determinations, scan type and wavelength of radiation used is *ω* and 0.71073 Å, respectively.

Table 2. Summary of the $^{31}P\{^1H\}$ NMR Data of Pt_2[a]

	chemical shifts δ (ppm)			coupling constants (Hz)					
complex	P1	P2	P3	$^1J_{P1\text{-}Pt}$	$^1J_{P2\text{-}Pt}$	$^1J_{P3\text{-}Pt}$	$^2J_{P1\text{-}P2}$	$^2J_{P1\text{-}P3}$	$J_{P2\text{-}P3}$
1a	45.86	−23.26	−31.09	2828	2444	1461	361	11	39
1b	41.04	−23.75	−31.67	2812	2421	1464	361	11	39
2a	56.40	47.89	43.80	2741	2791	1765	347	4	10
2b	56.25	43.65	43.80	2717	2778	1765	347	6	13
3a	48.23	9.65	−5.09	2804	2707	1738	343	15	34
3b	44.82	10.66	−4.93	2783	2697	1741	347	15	34

[a] 121.5 MHz, in CD_2Cl_2 for **1a** and **1b**, in acetone-d_6 for **2a** and **2b**, in CD_3CN for **3a** and **3b**, $T = 300$ K.

was concentrated by rotaevaporation, and yellow products were precipitated by adding excess diethyl ether to the solution. Slow diffusion of Et_2O into a CH_2Cl_2 solution of the crude products gave a mixture of crystals of **2a** and **2b**, which could be separated, as the crystals of **2a** lost solvent easily and became opaque in the air in a few minutes while the crystals of **2b** remained transparent. The separated crystals of **2a** and **2b** were purified by repeated recrystallization from CH_2Cl_2/Et_2O. Total yield: 115 mg, 95%. Anal. Calcd (%) for **2a**·CH_2Cl_2 ($C_{92}H_{74}F_6O_6P_6Pt_2S_2 \cdot CH_2Cl_2$): C, 52.82; H, 3.62. Found (%): C, 53.22; H, 3.59. Calcd (%) for **2b**·$0.5CH_2Cl_2$ ($C_{92}H_{74}F_6O_6P_6Pt_2S_2 \cdot 0.5CH_2Cl_2$): C, 53.62; H, 3.65. Found (%): C, 53.76; H, 3.86. ^1H NMR (300 MHz, δ/ppm) for **2a** (in CD_3OD): 7.85–7.82 (m, 8H, Ph), 7.74–7.72 (m, 2H, $H_{5,8}$, An), 7.62–7.22 (m, 54H, Ph and $H_{2,3}$ of An), 7.04–7.01 (m, 2H, $H_{6,7}$, An), 2.54–2.34 (m, 8H, CH_2); **2b** (in CD_2Cl_2): 7.88–7.16 (unresolved multiplets, 64H, Ph and $H_{2,4,6,8}$ of An), 6.66–6.61 (m, 2H, $H_{3,7}$ of An), 2.36–2.28 (m, 8H, PCH_2). $^{31}P\{^1H\}$ NMR: see Table 2. ESI-MS (*m*/*z*): **2a** and **2b** 865.8 $[M - 2OTf]^{2+}$.

Syntheses of *syn*-/*anti*-[Pt_2(dppp)$_2$(PAnP-H$_2$)](OTf)$_2$ (3a,b). In a typical reaction, PAnP (33 mg, 0.060 mmol) was added to 40 mL of a CH_3CN/CH_2Cl_2 (1:1, v/v) solution of 2 molar equiv of Pt(dppp)$(OTf)_2$ (97 mg, 0.121 mmol), which was prepared *in situ*. The solution was stirred at room temperature overnight and then filtered. The filtrate was concentrated by rotaevaporation, and yellow products were precipitated by adding excess diethyl ether to the solution. The two isomers were separated by recrystallization. Slow diffusion of Et_2O into a CH_2Cl_2 solution of the crude products in a test tube gave crystals of **3a** and noncrystalline films of **3b** covering the test tube wall. The crystals of **3a** were separated, and the remaining was recrystallized. This process was repeated several times to obtain purified **3a** and **3b**. Single crystals of **3b** suitable for X-ray study were obtained by evaporating a saturated CH_2Cl_2/Et_2O solution of purified **3b**. Total yield: 110 mg, 90%. Anal. Calcd (%) for **3a** ($C_{94}H_{78}F_6O_6P_6Pt_2S_2$): C, 54.87; H, 3.82. Found (%): C, 54.99; H, 3.79. Calcd (%) for **3b**·$2H_2O$ ($C_{94}H_{78}F_6O_6P_6Pt_2S_2 \cdot 2H_2O$): C, 53.92; H, 3.95. Found (%): C, 53.93; H, 3.83. ^1H NMR (300 MHz, δ/ppm) for **3a** (in CD_3CN): 7.72–7.60 (m, 12H, Ph), 7.58–7.55 (m, 2H, $H_{5,8}$, An), 7.45–7.40 (m, 32H, Ph), 7.25–7.05 (m, 18H, Ph and $H_{2,3}$ of An), 7.01–6.95 (m, 2H, $H_{6,7}$, An), 2.48–2.40 (m, 8H, PCH_2), 1.90–1.73 (m, 4H, CCH_2C); **3b** (in CD_3CN): 7.82–7.76 (m, 8H, Ph), 7.69–7.63 (m, 2H, $H_{2,6}$, An), 7.52–7.24 (m, 38H, Ph and $H_{4,8}$ of An), 7.15–7.08 (m, 16H, Ph), 6.43–6.38 (m, 2H, $H_{3,7}$, An), 2.45–2.38 (m, 8H, PCH_2), 1.87–1.75 (m, 4H, CCH_2C). $^{31}P\{^1H\}$ NMR: see Table 2. ESI-MS (*m*/*z*): **3a** and **3b**, 879.8 $[M - 2OTf]^{2+}$.

Synthesis of [Pt(dppe)(PAn-H)]ClO_4 (4). To 20 mL of a dichloromethane solution of Pt(dppe)Cl_2 (140 mg, 0.211 mmol) was added 10 mL of an acetonitrile solution of $AgClO_4$ (87 mg, 0.421 mmol). The solution was stirred in the dark for 2 h and filtered. To the filtrate was added PAn (76 mg, 0.211 mmol). The mixture was stirred at room temperature for 2 h and then filtered. Addition of excess diethyl ether to the concentrated filtrate gave a pale yellow precipitate. The product was purified by recrystallization from diethyl ether/dichloromethane. Yield: 200 mg, 90%. Anal. Calcd (%) for $C_{52}H_{42}ClO_4P_3Pt$: C, 59.24; H, 4.01. Found (%): C, 59.43; H, 3.28. ^1H NMR (500 MHz, CD_2Cl_2, δ/ppm): 8.65 (d, 1H, H_{10}, An), 8.10 (d, 1H, H_5, An), 7.96–7.92 (m, 5H, H_2 of An and $H_{2,2'}$ and $H_{6,6'}$ of Ph_2P_1), 7.85 (dd, 1H, H_4, An), 7.67–7.64 (m, 2H, $H_{4,4'}$, Ph_2P_1), 7.60–7.57 (m, 4H, $H_{3,3'}$ and $H_{5,5'}$ of Ph_2P_1), 7.52 (d, 1H, H_8, An), 7.42–7.33 (m, 9H, H_6 of An and Ph of dppe), 7.25–7.18 (m, 13H, H_7 of An and Ph of dppe), 6.96–6.93 (m, 1H, H_3, An), 2.42–2.28 (m, 4H, CH_2). $^{31}P\{^1H\}$ NMR (121.5 MHz, CD_2Cl_2, δ/ppm): 54.82 (dd, P_1), 44.41 (dd, P_2), 42.16 (dd, P_3); $^1J(P_1-Pt) = 2746$ Hz, $^1J(P_2-Pt) = 2796$ Hz, $^1J(P_3-Pt) = 1751$ Hz; $^2J(P_1-P_2) = 347$ Hz, $^2J(P_1-P_3) = 8$ Hz, $J(P_2-P_3) = 15$ Hz. ESI-MS (*m*/*z*): 954.4 $[M - ClO_4]^+$.

Results and Discussion

Synthesis. Reacting PAnP with Pt(L)$(OTf)_2$ (L = dppm, dppe, and dppp) produced doubly cyclometalated complexes [Pt_2(L)$_2$(PAnP-H$_2$)](OTf)$_2$ (**Pt_2**) in high yields. The products obtained display cluster peaks attributable to the doubly charged $[(PtL)_2(PAnP\text{-}H_2)]^{2+}$ (L = dppm, dppe, or dppp) and the singly charged $[(PtL)_2(PAnP\text{-}H_2)OTf]^+$ in their ESI-MS spectra. A pair of geometrical isomers, *anti*- and *syn*-[Pt_2(L)$_2$(PAnP-H$_2$)](OTf)$_2$, are generated in each reaction (Scheme 1). The ratios of the two isomers were obtained from the $^{31}P\{^1H\}$ spectra of the crude products from the reactions in CH_3CN/CH_2Cl_2 (1:1, v/v). The double cyclometalation was regioselective, as the isomer ratios (*syn*/*anti*) were 77:37, 90:10, and 77:33 for L = dppm, dppe, and dppp, respectively. Pure *syn*-isomers **1a**, **2a**, and **3a** and *anti*-isomers **2b** and **3b** were isolated by fractional recrystallization. The $^{31}P\{^1H\}$ NMR spectra of the **Pt_2** complexes are similar; each spectrum consists of three mutually coupled double-doublets, each flanked with two Pt satellites. The signals were assigned on the basis of the coupling constants $^2J_{P\text{-}P}$ and $^1J_{Pt\text{-}P}$ and chemical shifts, which are listed in Table 2. Inspecting the coupling constants of the signals shows that two of the P atoms (P1, P2) in each complex show large $^2J_{P\text{-}P}$ of 343–361 Hz and $^1J_{Pt\text{-}P}$ of 2421–2828 Hz, which are diagnostic for two *trans*-oriented P atoms (see Scheme 1 for labeling of the P atoms).[26] The signals are further split by the nuclear spin of the third P atom (P3). The small $^2J_{P\text{-}P}$ (4–39 Hz) implies that the third P atom is *cis* to the two *trans*-oriented P atoms. It is noted that the $^1J_{Pt\text{-}P}$ constant (1461–1765 Hz) of P3 is relatively small, suggesting that it is *trans* to a strong σ-donor.[26] The P3 is therefore assigned to a P atom in L that is *trans* to the metalated carbon atom. As the P2 and P3 have similar chemical shifts, they should belong to L, and the P1 is the P atom of PAnP.

Reacting Pt(dppe)$(ClO_4)_2$ with 1 molar equiv of 9-(diphenylphosphino)anthracene (PAn) gives the mononuclear cyclometalated complex [Pt(dppe)(PAn-H)](ClO_4) (**4**). The $^{31}P\{^1H\}$ NMR spectrum of the complex shows a similar pattern to those of corresponding dimetalated **2a** and **2b**.

(26) (a) Allen, F. H.; Pidcock, A. *J. Chem. Soc. A* **1968**, 2700. (b) Appleton, T. G.; Clark, H. C.; Manzer, L. E. *Coord. Chem. Rev.* **1973**, *10*, 335.

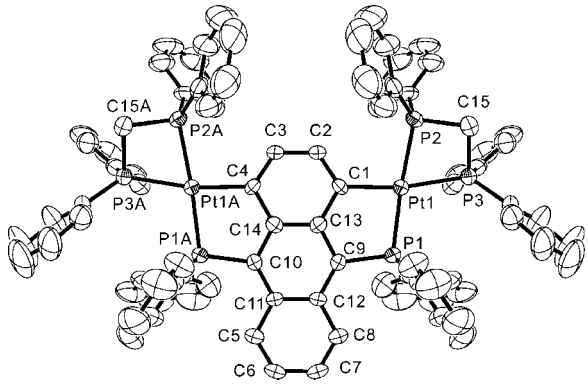

Figure 1. ORTEP diagram of **1a**·Et_2O (50% thermal ellipsoids). H atoms and anions are omitted for clarity.

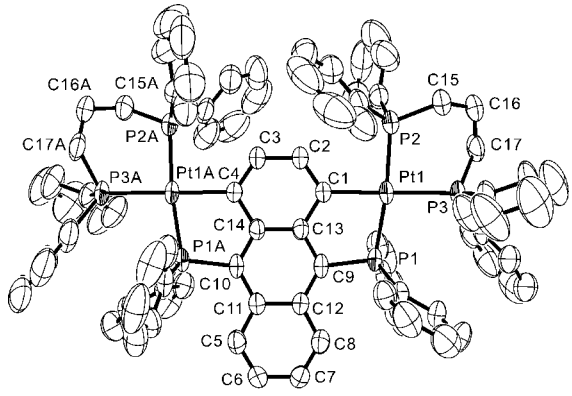

Figure 2. ORTEP diagram of **3a** (50% thermal ellipsoids). H atoms, solvent molecules, and anions are omitted for clarity.

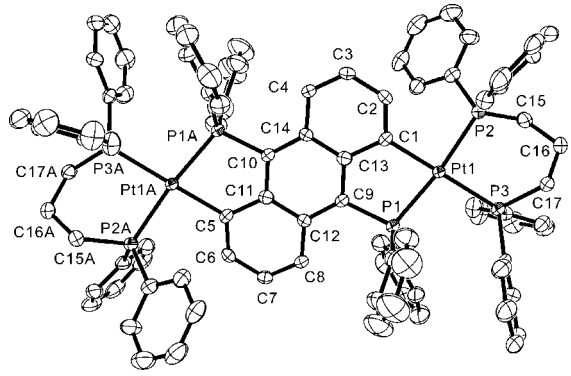

Figure 3. ORTEP diagram of **3b** (50% thermal ellipsoids). H atoms, solvent molecules, and anions are omitted for clarity.

Structures of the Cyclometalated Complexes. The X-ray crystal structures of *syn*-$[Pt_2(dppm)_2(PAnP\text{-}H_2)](OTf)_2 \cdot Et_2O$ (**1a**·Et_2O) (Figure 1), *syn*-$[Pt_2(dppe)_2(PAnP\text{-}H_2)](OTf)_2 \cdot 1.25CH_2Cl_2 \cdot 0.5Et_2O$ (**2a**·$1.25CH_2Cl_2 \cdot 0.5Et_2O$), *anti*-$[Pt_2(dppe)_2(PAnP\text{-}H_2)](OTf)_2 \cdot 2CH_2Cl_2$ (**2b**·$2CH_2Cl_2$) (the ORTEP diagrams of **2a** and **2b** are included in the Supporting Information), *syn*-$[Pt_2(dppp)_2(PAnP\text{-}H_2)](OTf)_2 \cdot 4.5CH_2Cl_2$ (**3a**·$4.5CH_2Cl_2$) (Figure 2), and *anti*-$[Pt_2(dppp)_2(PAnP\text{-}H_2)](OTf)_2 \cdot 4CH_2Cl_2$ (**3b**·$4CH_2Cl_2$) (Figure 3) were determined. Selected bond distances and angles are listed in Tables 3, 4, and 5. The structures of **1a**, **2a**, and **3a** are similar, showing two *syn*-oriented Pt centers attached to the C_1 and C_4 positions of the anthracenyl ring. On the other hand, the C_1 and C_5 positions are metalated in the *syn*-isomers **2b** and **3b**. The immediate coordination spheres of the *syn*- and *anti*-isomers are slightly deviated from idealized

Table 3. Selected Bond Lengths (Å) and Angles (deg) for 1a·Et_2O

Pt(1)−P(1) 2.2701(17)	P(1)−Pt(1)−P(2)173.83(7)
Pt(1)−P(2) 2.3163(17)	P(1)−Pt(1)−P(3)106.12(6)
Pt(1)−P(3) 2.3252(18)	P(2)−Pt(1)−P(3)70.74(6)
Pt(1)−C(1) 2.043(6)	P(1)−Pt(1)−C(1)83.78(17)
	P(2)−Pt(1)−C(1)99.68(17)
	P(3)−Pt(1)−C(1)169.69(18)

Table 4. Selected Bond Lengths (Å) and Angles (deg) for 3a·$4.5CH_2Cl_2$

Pt(1)−P(1) 2.2801(16)	P(1)−Pt(1)−P(2)173.21(5)
Pt(1)−P(2) 2.3279(18)	P(1)−Pt(1)−P(3)98.93(5)
Pt(1)−P(3) 2.3437(16)	P(2)−Pt(1)−P(3)87.49(5)
Pt(1)−C(1) 2.078(6)	P(1)−Pt(1)−C(1)80.83(14)
	P(2)−Pt(1)−C(1)92.80(14)
	P(3)−Pt(1)−C(1)178.96(18)

Table 5. Selected Bond Lengths (Å) and Angles (deg) for 3b·$4CH_2Cl_2$

Pt(1)−P(1) 2.2817(13)	P(1)−Pt(1)−P(2)171.79(5)
Pt(1)−P(2) 2.3257(13)	P(1)−Pt(1)−P(3)98.75(5)
Pt(1)−P(3) 2.3309(13)	P(2)−Pt(1)−P(3)86.88(5)
Pt(1)−C(1) 2.064(5)	P(1)−Pt(1)−C(1)80.86(15)
	P(2)−Pt(1)−C(1)93.75(15)
	P(3)−Pt(1)−C(1)177.70(16)

C_{2v} and C_{2h} symmetry, respectively. The Pt−P (2.2701(17)−2.3437(16) Å) and Pt−C (2.043(6)−2.106(1) Å) bond lengths in the complexes are similar and typical for cyclometalated Pt−phosphine complexes.[9c,17a] The anthracenyl rings are essentially planar. The metal centers show a distorted square-planar geometry and form two five-membered chelate rings with the two P atoms of PAnP and carbon atoms of the anthracenyl ring. In addition, the Pt atoms are chelated by dppm, dppe, and dppp in forming four- (**1a**), five- (**2a** and **2b**), and six-membered (**3a** and **3b**) rings, respectively. Expectedly, the bite angles P2−Pt1−P3 follow the order **1a** (70.74(6)°) < **2a** (83.83(13)°) and **2b** (82.99(6)°) < **3a** (87.49(5)°) and **3b** (86.88(5)°). As a consequence, the P2−Pt1−C1 angle in **3a** (92.80(14)°) is the smallest among all the complexes (cf. **1a**, 99.68(17)°).

As a result, the phenyl rings in **3a** are highly congested. The six-membered Pt(dppp) rings in **3a** adopt a twisted chair conformation, and the two phenyl rings on each P atom of dppp are oriented either axially or equatorially. The dihedral angle between the axial phenyl rings on P2 and the anthracenyl ring is 75.8°, whereas the corresponding angle for the equatorial phenyl rings on P2 are much smaller, being 49.3°. Because of the small dihedral and P2−Pt1−C1 angles, the equatorial phenyl rings in **3a** are close to the anthracenyl ring and are extended toward the opposite P2A atoms. To avoid severe steric repulsion, the axial phenyl rings of P2 are directed facing the equatorial phenyl rings of the P2A atom and vice versa.

Complex **4** (Figure 4, Table 6 for selected bond distances and angles) contains one Pt ion attached to the anthracenyl ring at the C_1 position. The coordination geometry and Pt−C and Pt−P bond lengths are similar to those of **2a** and **2b**.

Electronic Spectroscopy. The UV–vis absorption spectra of **4** and PAn (Figure 5) display moderately intense vibronic bands around 320–440 nm (the spectral data of $\mathbf{Pt_2}$ and **4** are summarized in Table 7). The shapes of the bands are similar, and the vibronic spacing in the band of **4** (1336 and 1350 cm^{-1}) is close to those of PAn (1336, 1329 cm^{-1}). The band of **4** is red-shifted from that of PAn by ~1200 cm^{-1}. In addition, the compounds display very intense absorption at 267 nm (**4**, $\varepsilon_{max} = 9.25 \times 10^4$ M^{-1} cm^{-1}) and 256 nm (PAn, $\varepsilon_{max} = 1.02 \times 10^5$ M^{-1} cm^{-1}).

Table 6. Selected Bond Lengths (Å) and Angles (deg) for 4·CH_2Cl_2

Pt(1)−P(1) 2.2922(11)	P(1)−Pt(1)−P(2)178.79(4)
Pt(1)−P(2) 2.3088(11)	P(1)−Pt(1)−P(3)97.58(4)
Pt(1)−P(3) 2.3222(11)	P(2)−Pt(1)−P(3)83.18(4)
Pt(1)−C(1) 2.077(4)	P(1)−Pt(1)−C(1)82.77(12)
	P(2)−Pt(1)−C(1)96.53(12)
	P(3)−Pt(1)−C(1)176.53(10)

The spectra of the binuclear complexes (Figures 6 and 7, see Table 7 for spectroscopic data) are different from that of **4**. The spectra of the *syn*-isomers **1a**, **2a**, and **3a** display two intense, overlapping absorption bands labeled A and B at 320–520 nm. The higher energy and more intense absorption band B is maximized around ~350–420 nm ($\varepsilon_{max} \approx (1.5-2) \times 10^4$ M^{-1} cm^{-1}) and the lower energy band A at ~430–500 nm ($\varepsilon_{max} \approx 1 \times 10^4$ M^{-1} cm^{-1}). Poorly resolved vibronic peaks could be discerned. The *anti*-isomers **2b** and **3b** also display two intense bands A and B in the same spectral range (300–500 nm). Both bands A and B show distinct vibronic peaks with spacing of ~1300 cm^{-1}, with the former being more intense than the latter. Comparing the spectra of the complexes shows that bands A of **2b** and **3b** are slightly higher in energy than those of **2a** and **3a**.

The band A of **Pt_2** is red-shifted from the lowest energy $^1(\pi^* \leftarrow \pi)$ transition of the parent ligand PAnP by ~2000 cm^{-1}. An intense high-energy band at 266–285 nm ($\varepsilon_{max} = (6.26-8.76) \times 10^4$ M^{-1} cm^{-1}) is observed in the spectra of the binuclear complexes and is slightly lower than the corresponding absorption of PAnP ($\varepsilon_{max} = 261$ nm, $\varepsilon_{max} = 7.92 \times 10^4$ M^{-1} cm^{-1}). All the absorption bands are insensitive to solvent polarity, as they are red-shifted by <100 cm^{-1} as the solvent is changed from CH_2Cl_2 to DMSO.

Spectral Assignments. The low-energy bands of **4** and PAn have similar vibronic spacing and band shapes, suggesting that both arise from an intraligand $\pi^* \leftarrow \pi$ transition. In fact, they resemble the spectrum of anthracene,[27] which displays a moderately intense vibronic band at 320–390 nm and a very intense band at 255 nm. The absorption features of anthracene arise from four electronic transitions, as shown by the unperturbed π-system in Scheme 2. The vibronic band arises from the LUMO ← HOMO ($^1B_{1u} \leftarrow {}^1A_g$) transition (from here onward, HOMO and LUMO refer to the highest occupied and lowest unoccupied π- and π^*-orbitals of the anthracenyl ring, respectively). In a first-order approximation, the LUMO ← HOMO−1 and LUMO+1 ← HOMO transitions, which have the same energy, give rise to two degenerate $^1B_{2u}$ excited states. Strong first-order configuration interactions between the states give rise to a high-energy $^1B_{2u}{}^+$ state and a low energy $^1B_{2u}{}^-$ state—the so-called "plus" and "minus" states.[27a,b,28] The very intense band at 250 nm corresponds to the $^1B_{2u}{}^+ \leftarrow {}^1A_g$ transition. On the other hand, the $^1B_{2u}{}^- \leftarrow {}^1A_g$ transition, which is slightly higher in energy than the $^1B_{1u} \leftarrow {}^1A_g$ transition ($^1B_{1u}$ is lower than $^1B_{2u}{}^-$ by ~1500 cm^{-1}),[29] is forbidden ($\varepsilon \approx 10^2$ M^{-1} cm^{-1}) and hidden under the latter.[27a,b,28] Given the similar spectra of **4** and anthracene, the 320–440 and 265 nm bands are assigned to $^1B_{1u} \leftarrow {}^1A_g$ and $^1B_{2u}{}^+ \leftarrow {}^1A_g$ transitions, respectively. The $^1B_{2u}{}^- \leftarrow {}^1A_g$ transition is not observed and could lie under the $^1B_{1u} \leftarrow {}^1A_g$ transition.

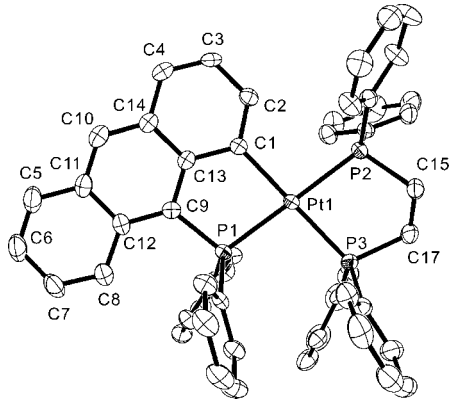

Figure 4. ORTEP diagram of **4** (50% thermal ellipsoids). H atoms, solvent, and the anion are omitted for clarity.

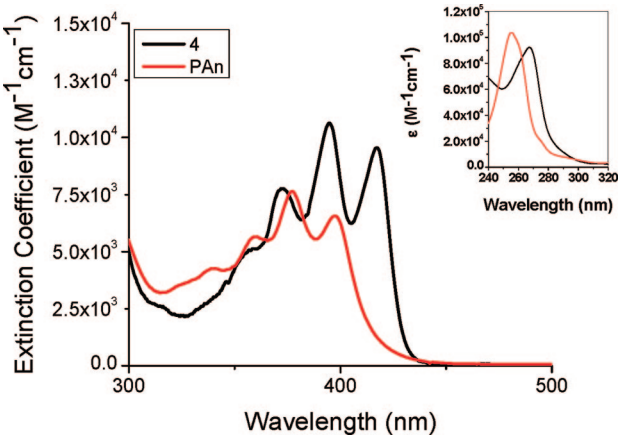

Figure 5. UV–vis absorption spectra of **PAn** and **4** in CH_2Cl_2. Shown in the inset are the bands at 240−320 nm.

Notably, the LUMO ← HOMO transition of **4** is red-shifted from that of PAn by ~1200 cm^{-1}. It is due to perturbation of the Pt ion on the π-system of the ligand (*vide infra*). Nonetheless, the "anthracene-like" spectrum of **4** indicates that the perturbation of a single Pt ion on the electronic structure of the anthracenyl ring is rather small.

On the other hand, the interactions between the two Pt ions and the π-system are apparently stronger in **Pt_2**. Unlike **4** and anthracene, the spectra of **Pt_2** show two bands A and B in the visible region. Given its energy and intensity, band A is assigned to the LUMO ← HOMO transition. The transition is red-shifted from those of **4** and the parental ligand PAnP by ~1200 and 2400 cm^{-1}, respectively. The LUMO ← HOMO transition of the *anti*-isomers shows distinct vibronic peaks. Notably, the 0–0 transitions (407 nm for **2b** and 409 nm for **3b**) are slightly more intense than the 0–1 transitions (381 nm for **2b** and 385 nm for **3b**). On the contrary, the 0–1 transitions are more intense than the 0–0 transitions for **4** and anthracene, suggesting that the anthracenyl framework is less distorted in the excited state of the *anti*-isomers than in that of **4** and anthracene. The very intense absorption around 260 nm corresponds to the $^1B_{2u}{}^+ \leftarrow {}^1A_g$ transition of anthracene. The bands B of **2b** and **3b** have similar vibronic spacing of ~1300 cm^{-1}, suggesting that the absorption is ligand-centered.

Spectroscopic studies showed that the π-system of anthracene could be significantly perturbed by substituents, especially the

(27) (a) Kessinger, M.; Michl, J. *Excited States and Photochemistry of Organic Molecules*; VCH: New York, 1995. (b) Suzuki, H. *Electronic Absorption Spectra, and Geometry of Organic Molecules; an Application of Molecular Orbital Theory*; Academic Press: New York, 1967. (c) Turro, N. J. *Modern Molecular Photochemistry*; Benjamin: Menlo Park, 1978.

(28) (a) Pariser, R. *J. Chem. Phys.* **1956**, *24*, 250. (b) Ham, N. S.; Ruedenberg, K. *J. Chem. Phys.* **1956**, *25*, 13.

(29) Kawashima, Y.; Hashimoto, T.; Nakano, H.; Hirao, K. *Theor. Chem. Acc.* **1999**, *102*, 49.

Table 7. Spectroscopic and Photophysical Data of Pt_2 and 4

complex	band A/nm (ε, 10^4 M^{-1} cm^{-1})	band B/nm (ε, 10^4 M^{-1} cm^{-1})	band C/nm (ε, 10^4 M^{-1} cm^{-1})	solution emission maxima/nm	Emission maxima at 77 K/nm	τ/ns[a]	fluorescence quantum yield Φ_f	k_R/ $\times$ 10^7 s^{-1}	k_{NR}/ $\times$ 10^8 s^{-1}
1a	434 (1.08), 460 (1.16)	346 (0.55), 365 (0.73), 382 (1.25), 405 (1.57)	266 (8.76)	510	503	1.7	0.055	3.24	5.56
2a	443 (1.13), 468 (1.08)	380 (1.43), 394 (1.75)	273 (7.97) (s)	504	490	1.9	0.059	3.11	4.95
2b	430 (1.89), 457 (2.13)	347 (0.62), 364 (0.74), 381 (1.16), 407 (0.98)	285 (8.65)	466	459	1.8	0.021	1.17	5.44
3a	443 (1.00), 463 (1.01)	394 (1.26)	273 (6.26) (s)	523	506	0.6	0.009	1.50	16.52
3b	434 (1.72), 460 (1.86)	367 (0.66), 385 (0.86), 409 (0.89)	272 (7.60) (s)	477	464	0.4	0.019	4.75	24.53
4	355 (0.49), 373 (0.78), 395 (1.06), 417 (0.95)		267 (9.25)	454	447	[b]	0.0016		

[a] Measured in CH_2Cl_2 at 298 K. [b] The lifetime of the emissions is too short to be measured accurately.

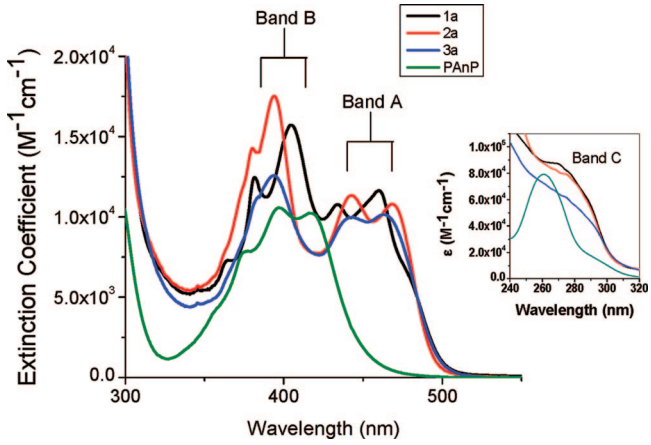

Figure 6. UV–vis absorption spectra of the *syn*-isomers and PAnP in CH_2Cl_2. Shown in the inset are the bands C.

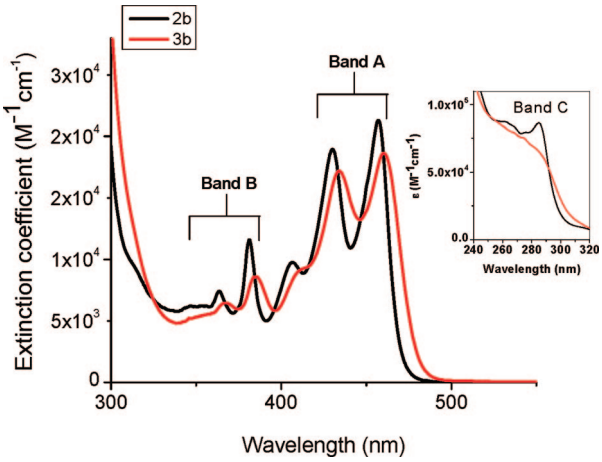

Figure 7. UV–vis absorption spectra of the *anti*-isomers in CH_2Cl_2. Shown in the inset are the bands C.

ones that exert a strong mesomeric effect.[30] The perturbation would lower the symmetry of the π-system, leading to a bathochromic shift of the LUMO ← HOMO transition and, more important, observation of the otherwise forbidden $^1B_{2u}^- \leftarrow {}^1A_g$ transition. The Pt ions in the dicyclometalated complexes could influence the π-system by their inductive effect and via π-interactions. Longuet-Higgins and Coulson pointed out that substitution of a H atom in an alternant aromatic ring would affect the Coulomb integral α_t of the $2p_z$-orbital of the substituted carbon atom i.[31] The effect propagates along the π-system and changes the energy of the molecular orbitals. According to first-order perturbation theory, the change in the energy of a molecular orbital R (δE_R) is related to the change in Coulomb integral ($\delta\alpha$) by the equation $\delta E_k = \sum_i c_{ik}^2 \delta\alpha_i$ where c_{ik} is the linear-combination-of-atomic-orbital (LCAO) coefficient of the $2p_z$-orbital of the substituted carbon atom i in molecular orbital k. It is reasonable to expect the potential field of the Pt ions would stabilize the ligand orbitals; that is, $\delta\alpha$ is negative. Semiempirical calculation on a model for PAnP shows that the LCAO coefficients for the $2p_z$-orbitals of the $C_{1/4/5/8}$ in the HOMO (0.29359) and LUMO (−0.27443) are close (see SF6 for the molecular orbitals of the model), as one would expect for alternant hydrocarbons. Accordingly, in a first-order approximation, the two orbitals should be stabilized almost equally by the potential field of the Pt ions; that is, $\delta E_{HOMO} \approx \delta E_{LOMO}$. It suggests that the inductive effect *alone* cannot cause the 2400 cm^{-1} shift of the LUMO ← HOMO transition.

Orbital interactions between the Pt ions and the anthracenyl ring mainly involve the metal dπ-orbitals and the HOMO and LUMO of the anthracenyl ring. For the *anti*-isomers in the idealized C_{2h} symmetry, the $1/\sqrt{2}$ ($d_{xz}^1 + d_{xz}^2$) (a_u) and $1/\sqrt{2}$ ($d_{xz}^1 - d_{xz}^2$) (b_g) orbitals can interact with the LUMO (a_u) and HOMO (b_g), respectively. Because of the stabilization of the dπ-orbitals by the π-accepting phosphines, it is reasonable that the metal orbitals are lower in energy than the HOMO, and accordingly the interactions would destabilize the HOMO and LUMO. The change in the energy of the orbitals, δE, is inversely proportional to the energy difference between the metal and ligand orbitals.[32] As the metal orbitals are closer in energy to the HOMO than to the LUMO, the former should be more destabilized than the latter. Similarly, the $1/\sqrt{2}$ ($6p_z^1 + 6p_z^2$) (a_u) and $1/\sqrt{2}$ ($6p_z^1 - 6p_z^2$) (b_g) orbitals of the Pt ions can overlap with the ligand orbitals. As the HOMO and LUMO are lower in energy than the $6p_z$-orbitals, both of them would be stabilized by the interactions, with the latter being more stabilized than the former, as it is closer in energy to the $6p_z$-orbitals. Collectively, the π-interactions reduce the HOMO−LUMO energy gap. It accounts for the red-shift of the LUMO ← HOMO observed in the cyclometalated complexes. Since the inductive effect and π-interactions are additive, the π-system of **Pt_2** is more perturbed than that of **4**. Both inductive effects and π-interactions do not alter the energy of the HOMO−1 and LUMO+1, as the orbitals have nodes at the substituted positions.

(30) (a) Baba, H.; Suzuki, S. *J. Chem. Phys.* **1961**, *35*, 1501. (b) Tichý, M.; Zahradník, R. *J. Phys. Chem.* **1969**, *73*, 534. (c) Rotkiewicz, K.; Grabowski, Z. R. *Trans. Faraday Soc.* **1969**, *65*, 3263. (d) Steiner, R. P.; Michl, J. *J. Am. Chem. Soc.* **1978**, *100*, 6861.

(31) Longuet-Higgins, H. C.; Coulson, C. A. *J. Chem. Soc.* **1949**, 971.

(32) Creutz, C.; Newton, M. D.; Sutin, N. *J. Photochem. Photobio. A* **1994**, *82*, 47.

Scheme 2. Left: HOMOs and LUMOs of anthracene. The red, blue, green, and black arrows represent the LUMO ← HOMO, LUMO ← HOMO−1, LUMO+1 ← HOMO, and LUMO+1 ← HOMO−1 transitions, respectively. Right: Ground state and four singlet excited states arising from the four electronic transitions (ref 27a)

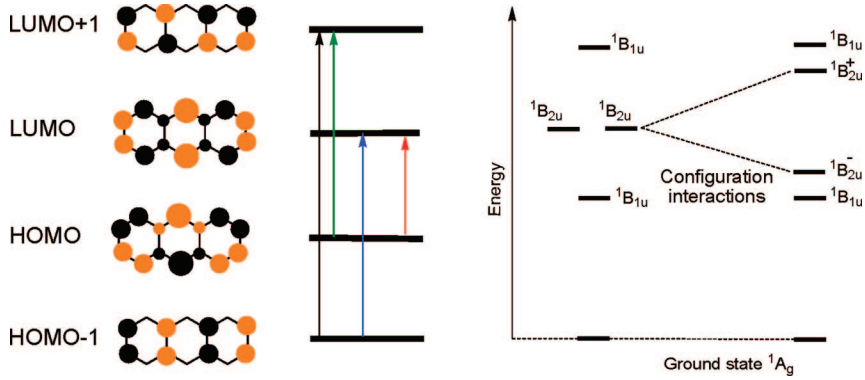

Scheme 3

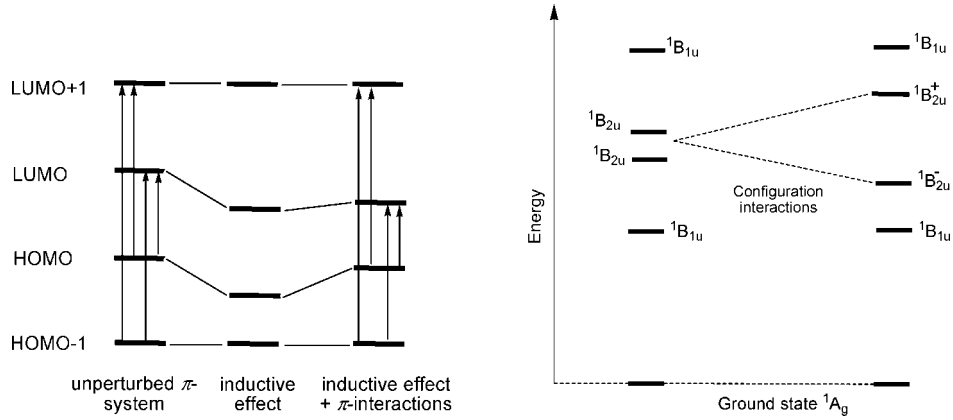

Scheme 3 shows the perturbed electronic structures (left) and singlet excited states (right) of **Pt_2**.

Electronic transitions from the HOMOs to the LUMOs in **Pt_2** give rise to four singlet excited states. The major difference between **Pt_2** and the unperturbed systems is that the degeneracy of the LUMO ← HOMO and LUMO+1 ← HOMO−1 transitions is removed by the metal–ligand interactions. In other words, the two $^1B_{2u}$ states are no longer degenerate. Consequently, configuration interactions between them become weaker and the splitting of the "plus" and "minus" states should be smaller than the one in the unperturbed systems. The bands B and C of **Pt_2** should correspond to the $^1B_{2u}^-$ ← ^1A_g and $^1B_{2u}^+$ ← ^1A_g transitions in the unperturbed systems, respectively.[33] For the unperturbed systems, the $^1B_{1u}$ ← ^1A_g (LUMO ← HOMO) and $^1B_{2u}^-$ ← ^1A_g transitions are close in energy and the latter is hidden under the intense former band. However, the energy gap between the two transitions is widened in the **Pt_2** because of the reduced configuration interactions and the red-shift of the LUMO ← HOMO transition. Taking the first peaks of bands A and B as the 0–0 transitions, the energy difference between the bands is estimated to be ∼4200 cm^{-1}, which is larger than the corresponding separation of ∼1500 cm^{-1} in anthracene. While the $^1B_{2u}^-$ ← ^1A_g transition is forbidden in the unperturbed systems, it is allowed in **Pt_2** because the two $^1B_{2u}$ states are no longer degenerate. This explains the high intensity of the band B.

No distinct MLCT absorption band can be discerned in the spectra. Studies on Pt−polypyridyl complexes showed that the extinction coefficients of the π^*(polypyridyl) ← 5d(Pt) charge-transfer transitions are ∼10^3 M^{-1} cm^{-1}.[4b,9c,12d,17a,34] Possibly the MLCT transitions in the present cyclometalated complexes are masked by the far more intense intraligand transition. It should be mentioned that the anthracenyl ring is also perturbed by the two PPh_2 groups at the C9 and C10 positions. However the effect is small, as the LUMO ← HOMO transition in PAnP is only red-shifted from that of anthracene by ∼1000 cm^{-1}. Accordingly, the strong perturbation observed in the spectra of **Pt_2** should be mainly due to the Pt ions.

Emission Spectroscopy. All of the cyclometalated complexes are emissive in degassed CH_2Cl_2 solution at room temperature (Figure 8a, the photophysical data are summarized in Table 7). The emission energies follow the order **4** > **2b**, **3b** > **1a**, **2a**, and **3a** and are parallel with the energy of band A of the complexes. The **Pt_2** complexes (λ_{max} = 466–523 nm, Φ = 0.009–0.059) are more emissive than **4** (λ_{max} = 454 nm, Φ = 0.0016). The emission bands of **2b**, **3b**, and **4** show a vibronic shoulder at a frequency of ∼1200 cm^{-1}. On the other hand, the emissions of the three *syn*-isomers (λ_{em} = 502–522 nm) are structureless. The emission lifetime (τ) of **Pt_2** is in the range of a nanosecond (0.4–1.9 ns). On the other hand, the emission lifetime of **4** is too short to be determined accurately. All excitation spectra resemble the corresponding absorption spectra, confirming that the emissions originate from the complexes.

All of the emissions become more intense and are slightly blue-shifted in the frozen glass solutions of the complexes at

(33) The $^1B_{1u}$ ← ^1A_g, $^1B_{2u}^-$ ← ^1A_g, and $^1B_{2u}^+$ ← ^1A_g transitions in the unperturbed systems correspond to $^1B_1$ ← $^1A_1$, $^1A_1^-$ ← $^1A_1$, and $^1A_1^+$ ← $^1A_1$ transitions in the C_{2v} *syn*-isomers and ^1B_u ← ^1A_g, $^1B_u^-$ ← ^1A_g, and $^1B_u^+$ ← ^1A_g transitions in the C_{2h} *anti*-isomers, respectively.

(34) (a) Connick, W. B.; Henling, L. M.; Marsh, R. E.; Gray, H. B. *Inorg. Chem.* **1996**, *35*, 6261. (b) Lai, S.-W.; Chan, M. C. W.; Cheung, K.-K.; Che, C.-M. *Inorg. Chem.* **1999**, *38*, 4262. (c) Du, P.; Schneider, J.; Jarosz, P.; Eisenberg, R. *J. Am. Chem. Soc.* **2006**, *128*, 7726. (d) Yam, V. W.-W.; Wong, K. M.-C.; Zhu, N. *J. Am. Chem. Soc.* **2002**, *124*, 6506.

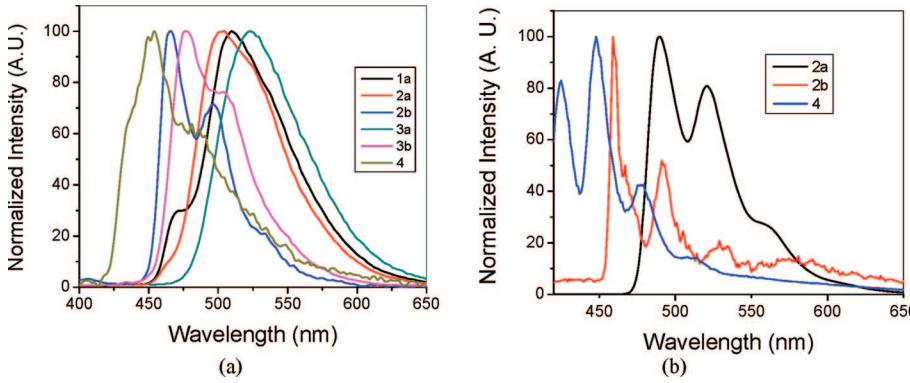

Figure 8. (a) Emission spectra of degassed CH_2Cl_2 of the Pt complexes at 298 K. (b) Emission spectra of glassy solutions (MeOH/EtOH = 1:4) of **2a**, **2b**, and **4** at 77 K.

77 K. The vibronic structures of the emissions of **2b**, **4** (Figure 8b), and **3b** (see Supporting Information) become more distinct. The vibronic spacing between the first two peaks for **2b**, **3b**, and **4** is 1420, 1300, and 1230 cm^{-1}, respectively. The three *syn*-isomers **1a**, **3a** (see Supporting Information), and **2a** (Figure 8b) show similar emission (λ_{max} = 490–506 nm) with a vibronic shoulder separated from the peak by ~1300 cm^{-1}.

Photophysics. The emissions of **Pt₂** have short lifetimes (τ = 0.4−1.9 ns) and small Stokes shifts, indicating that the emissions are fluorescent. In addition, rates of radiative decay k_R ((1.17–4.75) × 10^7 s^{-1}, Table 7) for the complexes are similar to those determined for fluorescence of anthracenes (e.g., k_R for anthracene = 6.33 × 10^7 s^{-1}).[35] All these indicate that the emissions arise from the lowest energy singlet excited states S_1 (corresponds to the $^1B_{1u}$) to the ground state S_0 (^1A_g). Huang–Rhys factors, which are approximated by the ratio of the 0−0 and 0−1 transitions,[36] are 1.2 for **4** and 0.5–0.83 for **Pt₂**. The lower Huang–Rhys factor for **Pt₂** implies the anthracenyl rings in the complexes are less distorted in the S_1 excited state than that of **4**. A possible reason is that the **Pt₂** complexes are more rigid than **4**. In addition, the small excited-state distortion of the **Pt₂** could be partly due to stronger MLCT character in the S_1 state of the complexes.

Previous studies on the photophysics of anthracenes identified three nonradiative decay pathways for S_1, namely, internal conversion from S_1 to S_0 ($S_1 \rightarrow S_0$) and intersystem crossing from S_1 to two triplet states T_1 and T_2 ($S_1 \rightarrow T_1$ and $S_1 \rightarrow T_2$).[35,37] Because of the large energy gap between S_1 and S_0 and the rigid molecular scaffolds, the rate of the internal conversion $k_{S1\text{-}S0}$ is slow ($k_{S1\text{-}S0}$ for anthracene is ~10^6 s^{-1}). The T_1 state, which arises from the LUMO ← HOMO transition, is much lower energy than the S_1 because of the large exchange integral. For instance, the S_1−T_1 gap is 1.2 × 10^4 cm^{-1} for anthracene.[35] This leads to an unfavorable Franck–Condon factor for the $S_1 \rightarrow T_1$ intersystem crossing and hence low intersystem crossing rate $k_{S1\text{-}T1}$. Lastly, there is an upper triplet state T_2 ($^3B_{1g}$ or $^3B_{1u}$) that is very close to S_1 in energy. Because of the small energy gap, the rate of the $S_1 \rightarrow T_2$ intersystem crossing (k_{ST}) is very high (~10^8−10^9 s^{-1}), and hence it is the major nonradiative decay pathway for the emissive S_1 state.[37] Depending on the substituents, T_2 could be higher or lower in energy than the S_1 state. In addition to the three ligand-centered excited states, the cyclometalated complexes have MLCT and ligand field excited states. However, the π-accepting phosphines should push these excited states up; accordingly they are expected to be higher in energy than S_1 and therefore do not contribute significantly to the nonradiative decay of the emissive state.

In principle, the Pt and P atoms in the complexes could increase the rate of spin-forbidden transitions such as the $S_1 \rightarrow T_1$ and $S_1 \rightarrow T_2$ intersystem crossing via their "heavy atom effect".[27] As these radiationless pathways compete with radiation decay, a direct consequence of the heavy atom effect is reduction of quantum yield of fluorescence Φ_f.[27,35] It is therefore reasonable to assume the effect is at least partially responsible for the exceptionally low Φ_f (0.0016) of **4** (cf. anthracene Φ_f = 0.27).[35] Having two Pt ions and two P atoms, the **Pt₂** complexes are expected to exhibit a stronger heavy atom effect than **4**. It is therefore surprising that the Φ_f values of the **Pt₂** (0.009–0.059) are higher than that of **4**. A similar anomaly has been observed: the Φ_f of 9,10-dibromoanthracene is found higher than that of 9-bromoanthracene.[37] The apparent absence of heavy atom effect in 9,10-bromoanthracene is due to a change in the order of the S_1 and T_2 energy. While the energy of S_1 (E_{S1}) is higher than the energy of T_2 (E_{T2}) in 9-bromoanthracene, the order is reversed in 9,10-dibromoanthracene, i.e., $E_{T2} > E_{S1}$. The $k_{S1\text{-}T2}$ is dependent on the S_1−T_2 gap, i.e., $k_{S1-T2} = k^o_{S1-T2} + A\exp(E_{S1} - E_{T2}/kT)$ (A is a constant and k^o_{S1-T2} is the intrinsic intersystem crossing rate).[38] Accordingly, the heavy atom effect, which would increase the $k_{S1-T2}{}^o$, is attenuated when $E_{T2} > E_{S1}$ (Scheme 4).

To determine the S_1−T_2 gap in **Pt₂** requires variable-temperature quantum yield measurements. Unfortunately the experimental setup is not available to us. Nonetheless, it is possible to gauge the heavy atom effect in the complexes by looking at the k_{S1-T2}. As mentioned, there are three major nonradiative decay pathways for the S_1, and hence $k_{NR} \approx k_{S0-S1} + k_{S1-T1} + k_{S1-T2}$. Accordingly, the k_{NR} can be taken as the upper limit of the k_{S1-T2} for the **Pt₂** complexes. The upper limits of k_{S1-T2} of **1a**, **b** and **2a**,**b** are similar (4.95–5.56 × 10^8 s^{-1}). More important, they are of the same order of magnitude as the k_{S1-T2} of 1.8 × 10^8 s^{-1} estimated for anthracene. The similar k_{S1-T2} suggests the heavy atom effect in the dinuclear complexes is subdued, possibly by a widened T_2−S_1 gap, as in the case of 9,10-dibromoanthracene. The estimated k_{NR} for **3a** (16.52 × 10^8 s^{-1}) and **3b** (24.53 × 10^8 s^{-1}) are higher than those for

(35) Birks, J. B. *Photophysics of Aromatic Molecules*"; Wiley: London, 1970.
(36) Miskowski, V. M.; Houlding, V. H. *Inorg. Chem.* **1991**, *30*, 4446.
(37) (a) Hiaryama, S.; Lampert, R. A.; Philips, D. *J. Chem. Soc., Faraday Trans. 2* **1985**, *81*, 371. (b) Robinson, G. W.; Frosh, R. P. *J. Chem. Phys.* **1962**, *37*, 1962.
(38) (a) Tanaka, M.; Tanaka, I.; Tai, S.; Hamanoue, K.; Sumitani, M.; Yoshihara, K. *J. Phys. Chem.* **1983**, *87*, 813. (b) Wu, K.-C.; Ware, W. R. *J. Am. Chem. Soc.* **1979**, *101*, 5906. (c) Dreeskamp, H.; Pabst, *J. Chem. Phys. Lett.* **1979**, *61*, 262.

Scheme 4. Radiative (→) and nonradiative (dashed arrow) pathways for the S_1 excited state

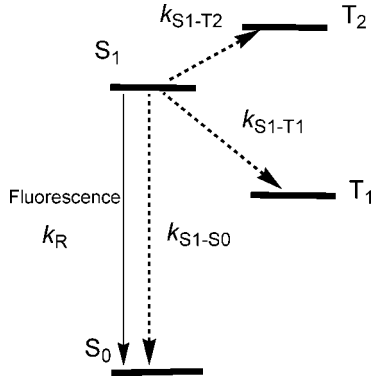

1a,**b** and **2a**,**b**. This is unlikely due to an increase in $k_{S1\text{-}T2}$ in **3a** and **3b**, as their electronic structures should be similar to other **Pt₂** complexes. Possibly the high k_{NR} is due to an increase in k_{S1-S0}, which could be due to motion of the flexible backbone (the so-called loose bolt effect)[39] and/or additional C−H bond stretching of dppp in **3a** and **3b**.[40]

(39) Guesten, H.; Mintas, M. Klasinc, L. *J. Am. Chem. Soc.* **1980**, *102*, 7936.

(40) (a) Kropp, J. L.; Windsor, M. W. *J. Chem. Phys.* **1965**, *39*, 2769. (b) King, C.; Auerbach, R. A.; Fronczek, F. R.; Roundhill, D. M. *J. Am. Chem. Soc.* **1986**, *108*, 5626.

Conclusion

Our spectroscopic study shows that the two Pt ions in the doubly cyclometalated complexes can alter the electronic structure of the anthracenyl ring significantly. The spectra of the complexes display two intense absorption bands in the visible region that correspond to the transitions in the unperturbed systems. The observation of the otherwise forbidden transition is due to the removal of the degeneracy of the excited states by metal–ligand interactions. All of the cyclometalated complexes display intraligand fluorescence from their S_1 excited states. There is an apparent absence of heavy atom effects on the S_1-T_2 intersystem crossing in the dicyclometalated complexes, which is possibly due to a widened gap between the S_1 and T_2 states.

Acknowledgment. We thank Dr. Koh Lip Lin and Ms. Tan Geok Kheng for solving the X-ray crystal structures of the compounds, and National University of Singapore for financial support. K.-Y.W. acknowledges support from the Hong Kong Polytechnic University.

Supporting Information Available: CIF files for **1a**, **2a**, **2b**, **3a**, **3b**, and **4**. X-ray crystal structures and selected bond lengths and angles for **2a** and **2b**. Emission spectra of **1a**, **3a**, and **3b** in glassy solutions at 77 K. Semiempirical molecular orbital diagram of a model compound for PAnP. This material is available free of charge via the Internet at http://pubs.acs.org.

OM700706R